Supplementary Information for

Hyper-activation of HUSH complex function by Charcot-Marie-Tooth disease mutation in *MORC2*

Iva A. Tchasovnikarova[1,2†], Richard T. Timms[1†], Christopher H. Douse[3], Rhys C. Roberts[4], Gordon Dougan[5], Robert E. Kingston[2], Yorgo Modis[3] and Paul J. Lehner[1*]

[1]Department of Medicine, Cambridge Institute for Medical Research, Cambridge Biomedical Campus, Cambridge, CB2 0XY, UK

[2]Department of Molecular Biology, Massachusetts General Hospital, and Department of Genetics, Harvard Medical School, Boston, MA 02114, USA

[3]Department of Medicine, University of Cambridge, MRC Laboratory of Molecular Biology, Francis Crick Way, Cambridge Biomedical Campus, Cambridge, CB2 0QH, UK

[4]Department of Clinical Neurosciences, Cambridge Institute for Medical Research, Cambridge Biomedical Campus, Cambridge, CB2 0XY, UK

[5]Wellcome Trust Sanger Institute, Wellcome Trust Genome Campus, Hinxton, Cambridge, CB10 1SA, UK

Supplementary Figures

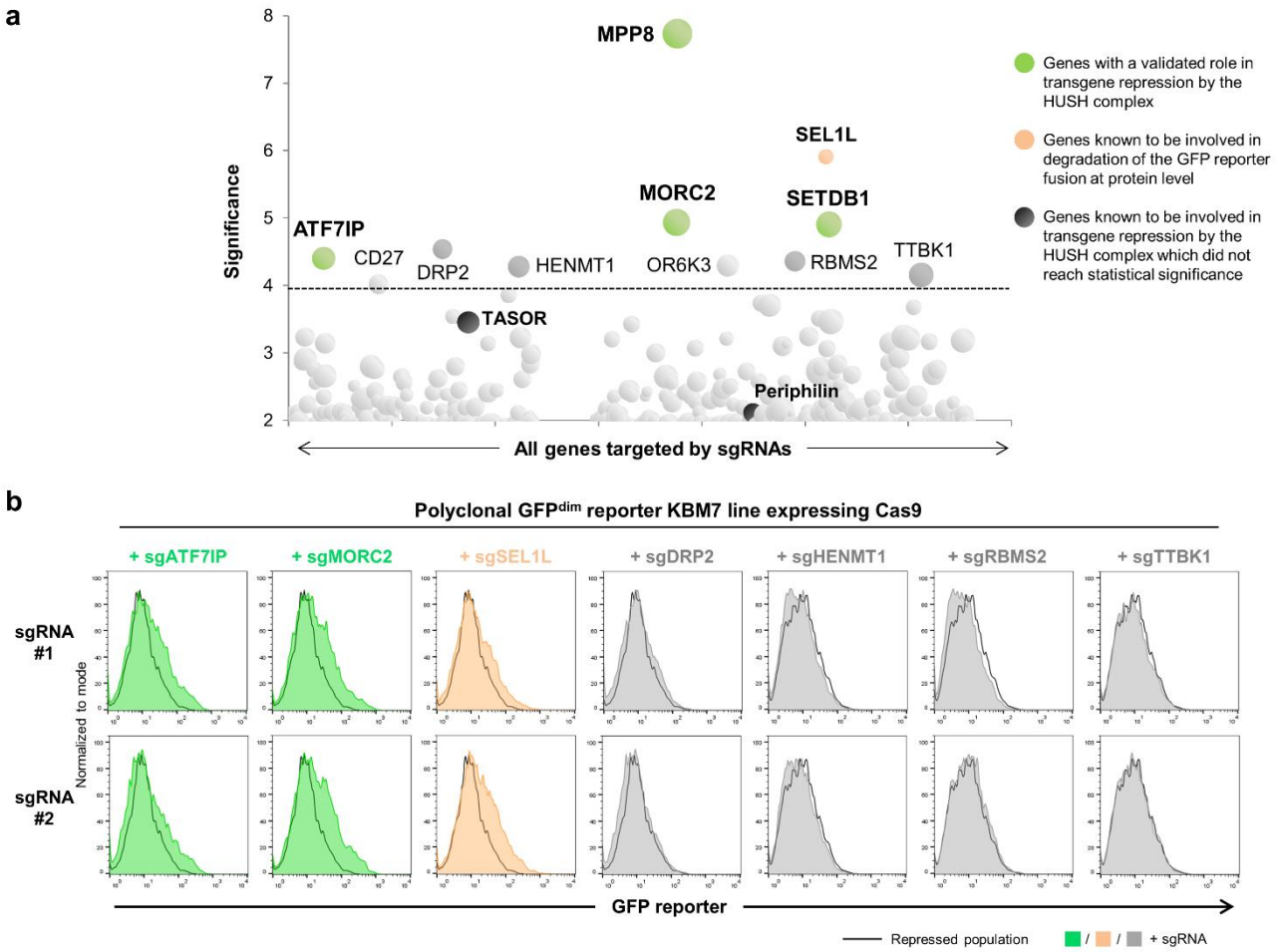

Supplementary Figure 1. Validating a role for candidate genes identified by the CRISPR screen in transgene silencing by the HUSH complex.

(a) Annotated bubble plot illustrating all of the potential hits from the CRISPR/Cas9-mediated forward genetic screen. All genes targeted by sgRNAs are arranged alphabetically on the x-axis. Bubble size is proportional to the number of active sgRNAs for each gene.

(b) Validation of candidate genes by individual CRISPR/Cas9-mediated gene disruption experiments. Two sgRNAs targeting each of the indicated candidate genes were designed for validation experiments; *CD27* and *OR6K3* were not included as they encode transmembrane proteins which localize to the plasma membrane. These sgRNAs were expressed together with Cas9 in the same polyclonal GFP^{dim} KBM7 cell line harboring HUSH-repressed transgenes, and derepression of the GFP reporter constructs monitored by flow cytometry. Disruption of three genes increased GFP levels: *ATF7IP*, which we previously found to be critical for HUSH-mediated repression[15], *SEL1L*, which mediates the degradation of the GFP reporter fusion protein[14], and *MORC2*, a novel gene involved in transgene repression.

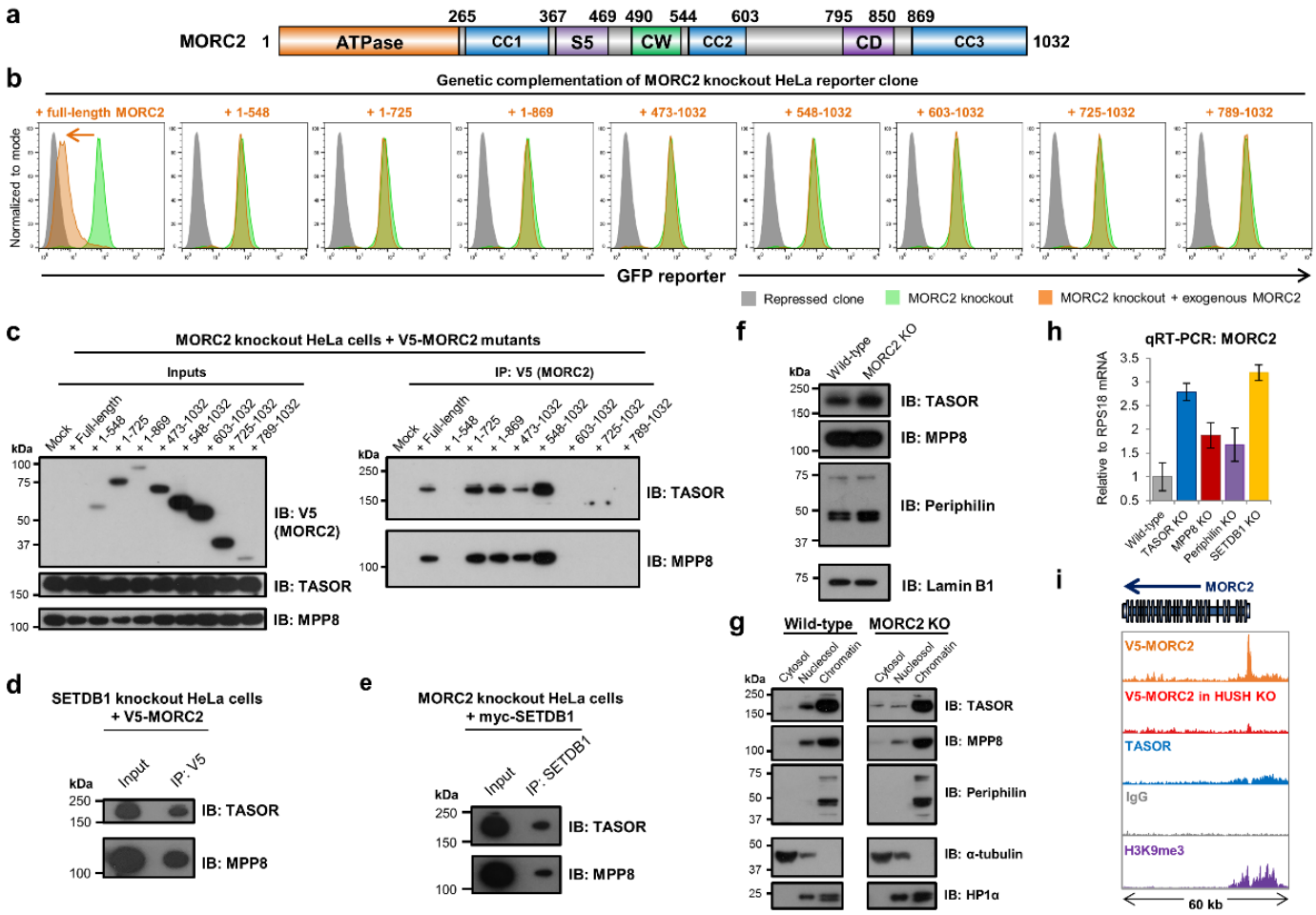

Supplementary Figure 2. MORC2, like SETDB1, does not appear to be a constitutive member of the HUSH complex.

(a-c) Assessing the domains of MORC2 required for the interaction with the HUSH complex. Schematic representation of the domain architecture of MORC2 (a). A panel of truncated V5-tagged MORC2 variants comprising the indicated residues were expressed in MORC2 knockout HeLa cells (see Supplementary Table 2 for full details). None of the MORC2 truncation mutants encoded a functional protein able to restore repression of the GFP reporter transgene (b). In order to assess the ability of the mutants to associate with the HUSH complex, the exogenous proteins were immunoprecipitated using an antibody against an N-terminal V5 epitope tag and co-immunoprecipitation of the HUSH subunits TASOR and MPP8 assayed by immunoblot (c). This analysis suggested that the second coiled-coil region (residues 548-603) of MORC2 was likely to be critical for interaction with the HUSH complex, with the caveat that although these mutant proteins are expressed in cells, we are unable to prove that they are correctly folded.

(d,e) Independent recruitment of MORC2 and SETDB1 by the HUSH complex. Co-immunoprecipitation experiments demonstrated that the interaction between MORC2 and the HUSH complex was preserved in SETDB1-null cells (d), while loss of MORC2 did not prevent the interaction between SETDB1 and the HUSH complex (e).

(f,g) Loss of MORC2 does not affect the levels of HUSH subunits nor their localization to chromatin. Immunoblot analysis comparing the levels of the HUSH subunits TASOR, MPP8 and Periphilin in wild-type versus MORC2 knockout cells (f). Subcellular fractionation comparing the localization of HUSH subunits in wild-type versus MORC2 knockout cells (g).

(h,i) The HUSH complex regulates MORC2 expression. Knockout of HUSH subunits or SETDB1 resulted in increased expression of MORC2 mRNA (h), while ChIP-seq analysis showed that HUSH recruited MORC2 to an H3K9me3-marked site in the *MORC2* promoter bound by TASOR (i).

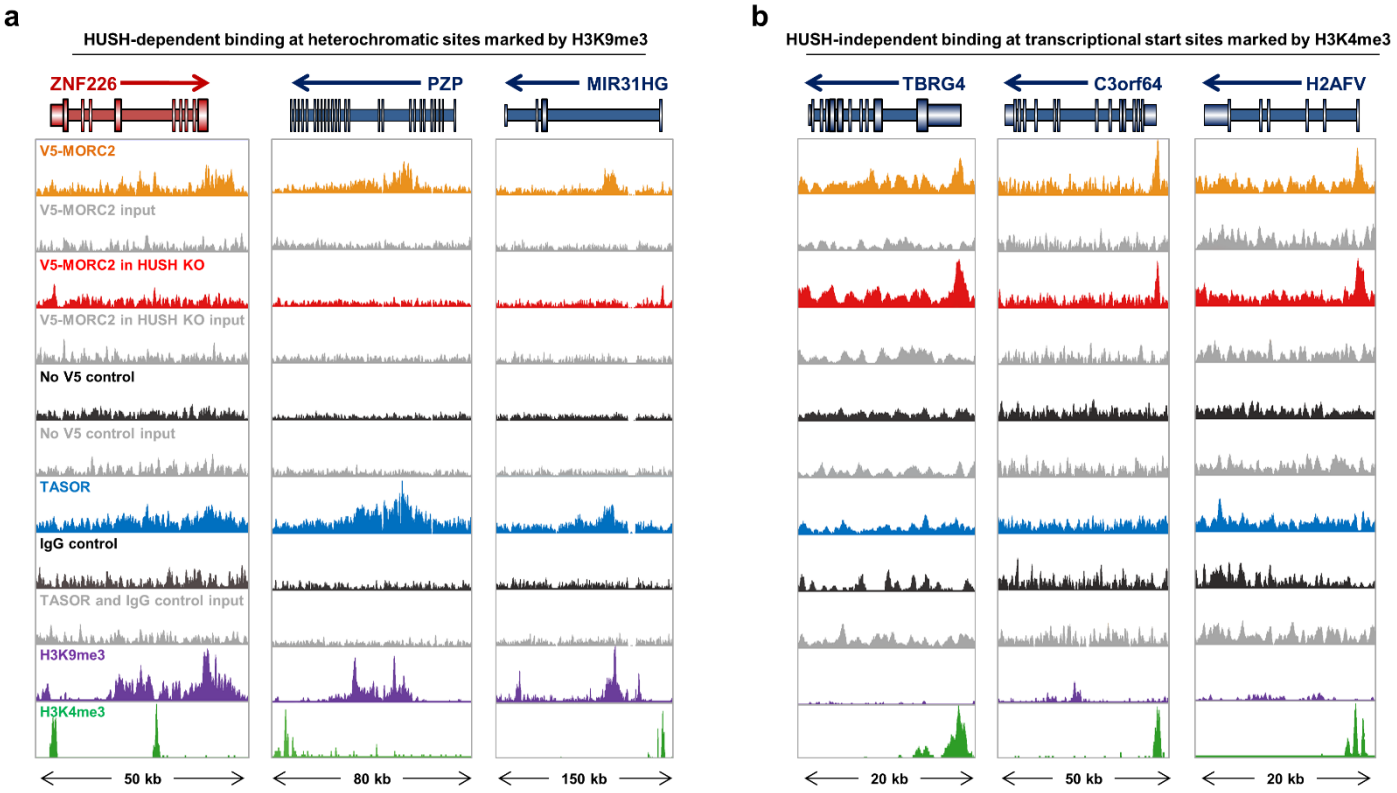

Supplementary Figure 3. Both HUSH-dependent and HUSH-independent mechanisms govern MORC2 to recruitment to target sites on chromatin.

(a,b) ChIP-seq data illustrating HUSH-dependent (a) and HUSH-independent (b) recruitment of MORC2 to target genomic loci. The full data for the six example loci depicted in Fig. 3 are shown, including input DNA control traces.

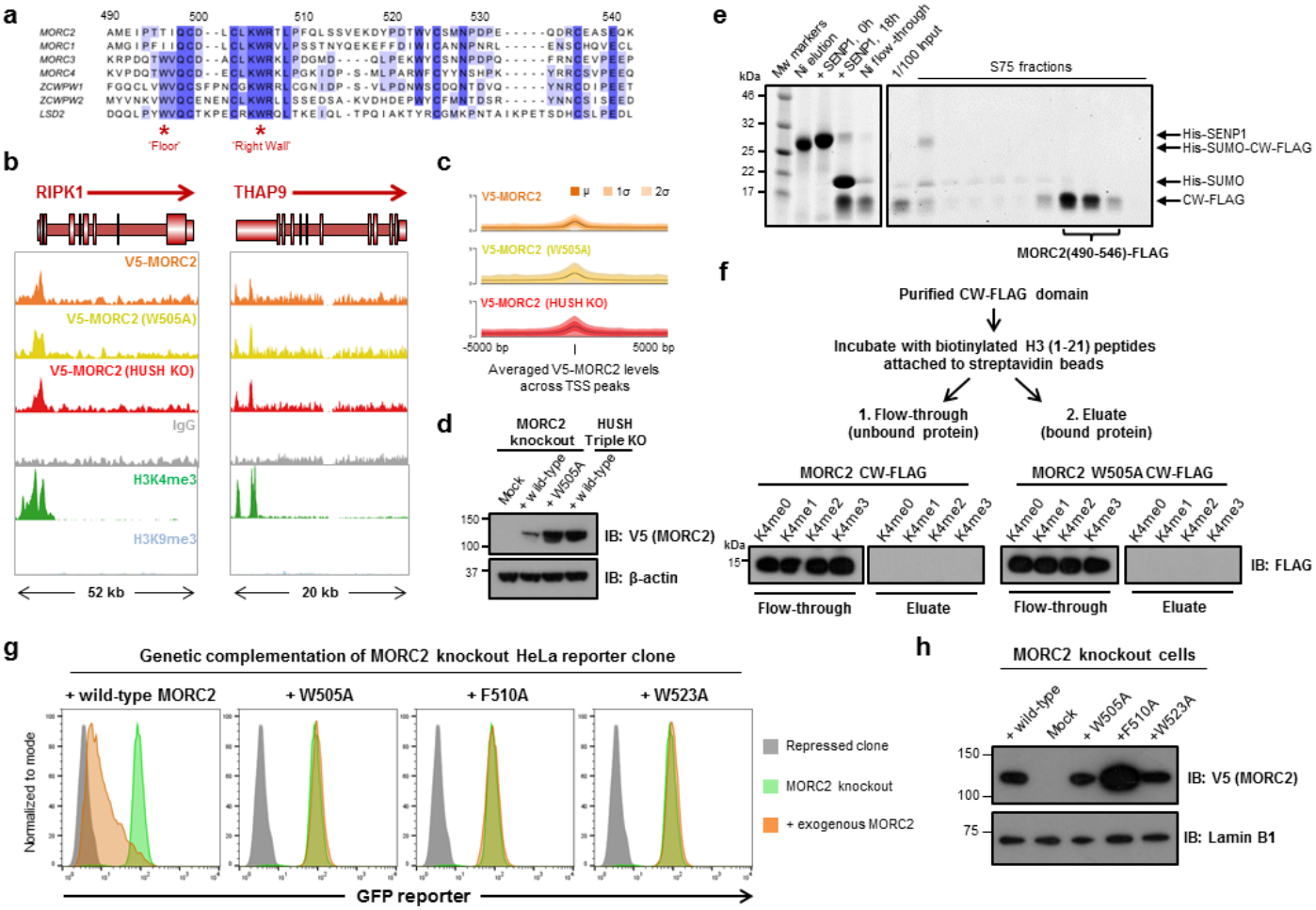

Supplementary Figure 4. The CW domain does not mediate MORC2 recruitment to transcriptional start sites marked by H3K4me3.

(a) Amino acid sequences of human CW domains. A multiple sequence alignment of the CW domains of seven human proteins is shown: MORC1-4, ZCWPW1 and 2[49], and LSD2[50]. Critical residues required for H3K4me3 recognition[20] are highlighted.

(b-d) MORC2 occupancy at transcriptional start sites (TSSs) is unaffected by mutation of the W505 residue in the CW domain. The recognition of H3K4me3 by the CW domains of MORC3[20] and ZCWPW1[49] is dependent on a conserved tryptophan residue corresponding to W505 in MORC2, but mutation of this residue to alanine (W505A) does not impair MORC2 occupancy at TSSs. Two example loci are shown (b), together with summary traces across all MORC2-bound TSS loci (c). Expression of the MORC2 W505A mutant protein was validated by immunoblot (d).

(e,f) The CW domain of MORC2 does not bind H3 peptides methylated at K4 *in vitro*. The CW domain of MORC2 with a C-terminal FLAG tag was expressed and purified from *E. coli* (e) and binding to biotinylated H3 peptides differentially methylated at K4 assessed by a pull-down assay followed by immunoblot (f).

(g,h) The aromatic residues of the CW domain are critical for HUSH function. Although the aromatic cage of the MORC2 CW domain did not appear to mediate recognition of H3K4me3, it was critical for MORC2 function as point mutations in these residues abolished HUSH-mediated transgene repression (g). Expression of the mutant proteins was validated by immunoblot (h).

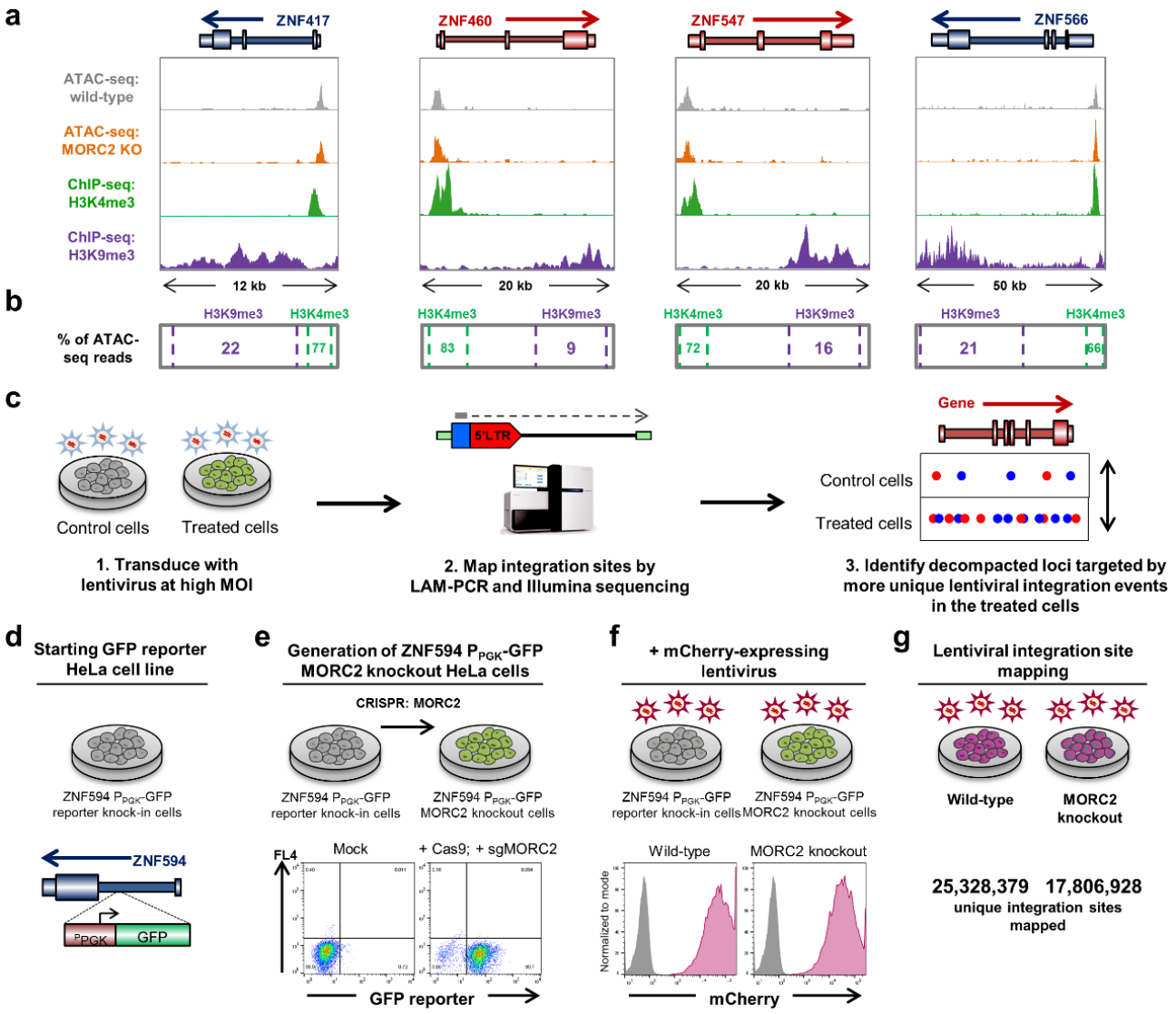

Supplementary Figure 5. Assessing chromatin decompaction in MORC2 knockout cells using ATAC-seq and Differential Viral Accessibility (DIVA).

(a,b) ATAC-seq yields insufficient coverage of the heterochromatic loci at which HUSH acts. Four example heterochromatic ZNF gene loci are shown (a). ATAC-seq was carried out in wild-type and MORC2 knockout HeLa cells, but the majority of the ATAC-seq reads fell at H3K4me3-marked transcriptional start sites and not across the gene bodies marked by H3K9me3 (b).

(c) Schematic overview of the DIVA approach. First, control and experimental cells were transduced with a lentiviral vector at a high multiplicity of infection, resulting in a large number of lentiviral integrations in each cell type. Linear amplification PCR (LAM-PCR) was then used to amplify the virus-genome junctions, allowing the mapping of the viral integration site through Illumina sequencing. Finally, the lentiviral integration sites in both samples were compared bioinformatically to identify genomic loci exhibiting decompaction that were more accessible to viral integration in the experimental cells as compared to the control.

(d-g) Exploiting DIVA to examine chromatin decompaction upon loss of MORC2. Beginning with a HeLa clone harboring a HUSH-repressed GFP reporter integrated in an intron of the *ZNF594* gene (d), we first created an isogenic MORC2 knockout line through CRISPR/Cas9-mediated gene disruption (e). Both the parental and MORC2 knockout cells were then transduced with a lentiviral vector at a high multiplicity of infection, which was monitored through expression of an mCherry transgene (f). Lastly, LAM-PCR and Illumina sequencing was used to map a large number of unique viral integration sites in each sample (g).

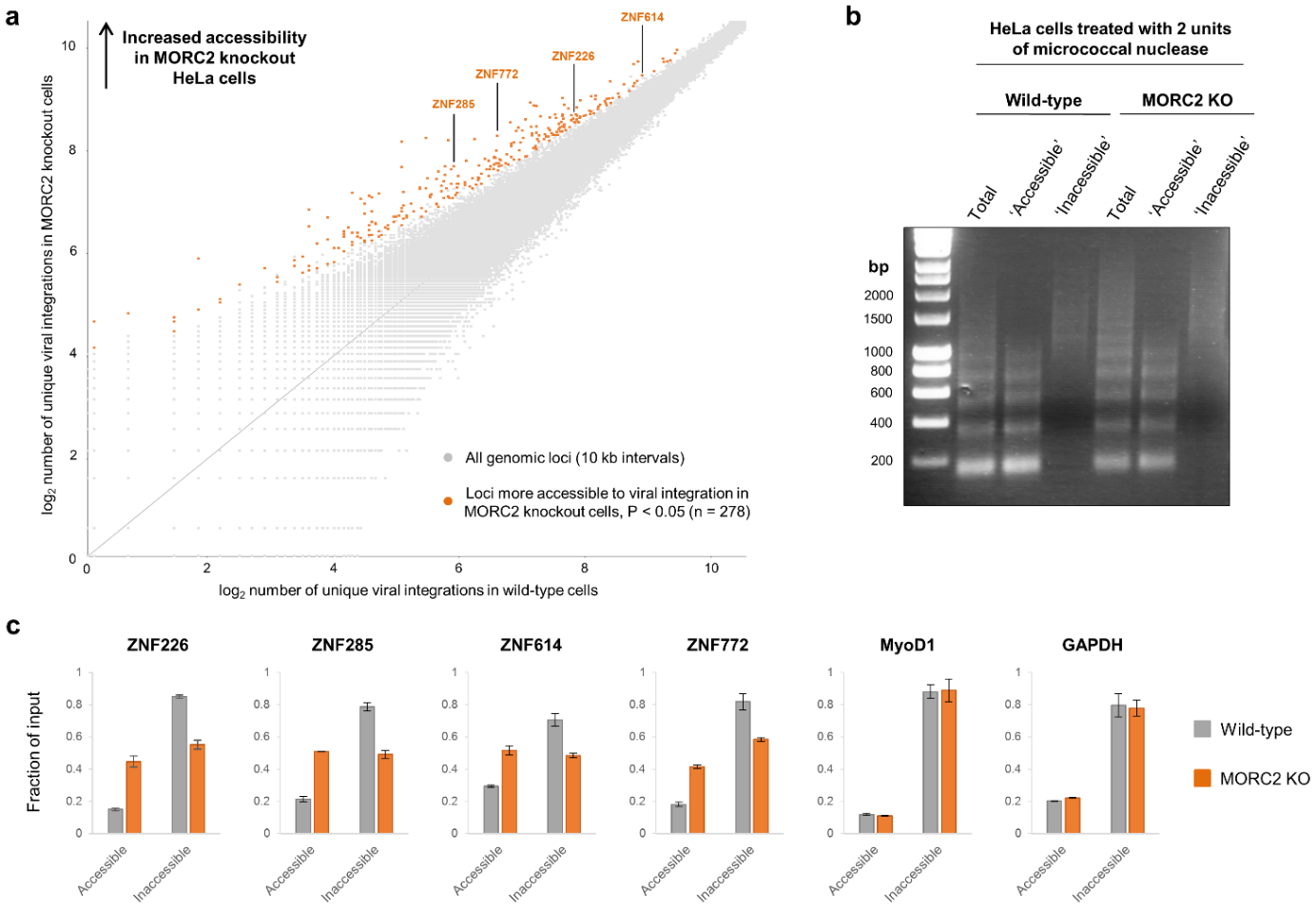

Supplementary Figure 6. Increased sensitivity to micrococcal nuclease digestion at HUSH target ZNF genes following disruption of MORC2.

(a) Four ZNF gene loci exhibiting decompaction upon loss of MORC2 were selected to validate the DIVA results.

(b,c) Validation of the DIVA data using a micrococcal nuclease sensitivity assay. Chromatin was digested with 2 units of micrococcal nuclease, and the digested DNA size-selected to yield an 'accessible' fraction (corresponding approximately to mono- to penta-nucleosomal fragments) and an 'inaccessible' fraction (comprising all larger fragments) (b). The amount of DNA from HUSH target sites in the 'accessible' versus the 'inaccessible' fraction in wild-type versus MORC2 knockout cells was then quantified by qPCR (c); the HUSH target ZNF gene loci were enriched in the accessible fraction and depleted in the inaccessible fraction in MORC2 knockout cells compared to the parental wild-type cells. MyoD1 and GAPDH, whose accessibility was not significantly altered in MORC2 knockout cells as measured by DIVA, were used as control loci.

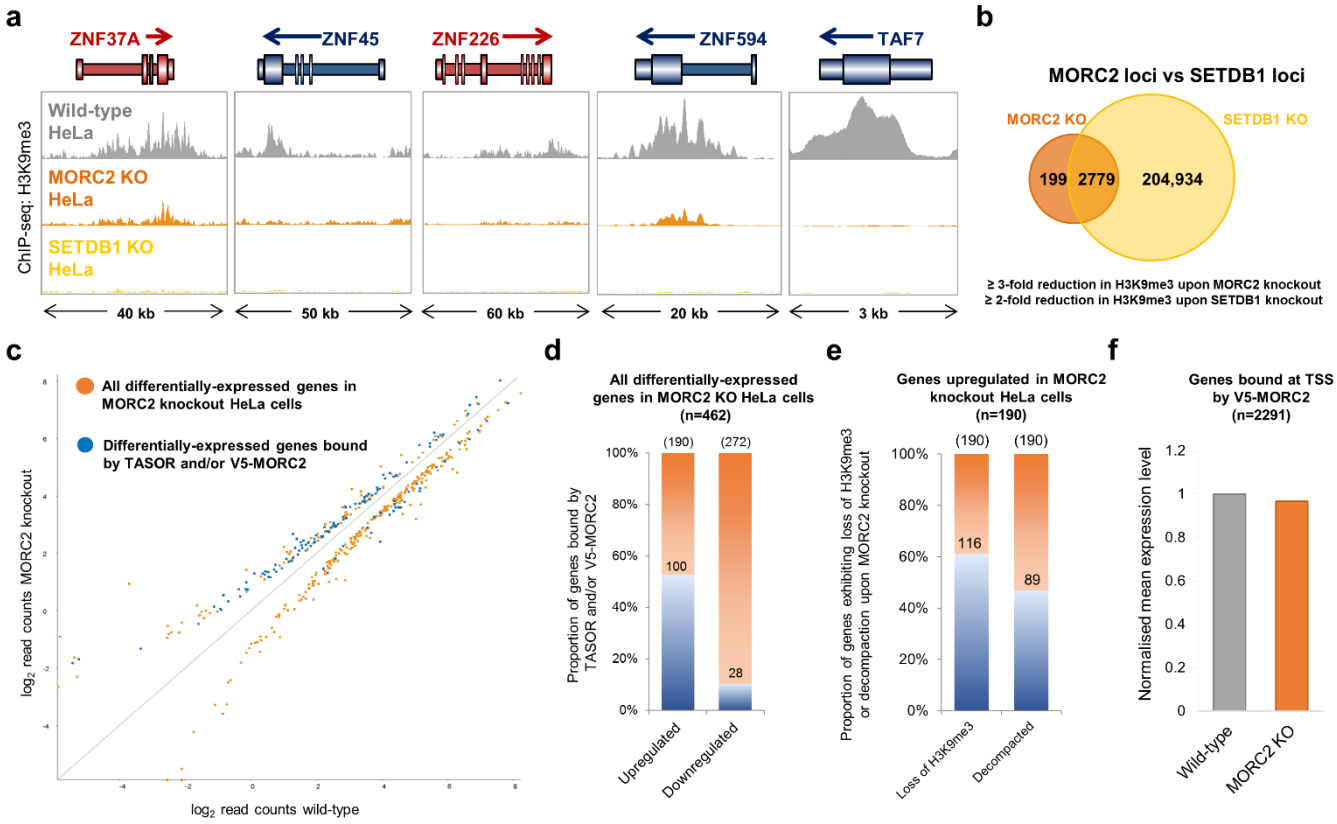

Supplementary Figure 7. Ablation of MORC2 results in a loss of H3K9me3 at HUSH target loci concomitant with transcriptional derepression.

(a) Loss of MORC2 results in decreased H3K9me3 at HUSH target loci. ChIP-seq for H3K9me3 was performed in wild-type, MORC2 knockout and SETDB1 knockout HeLa cells; five example heterochromatic loci are shown. H3K9me3 deposition across all of these loci is dependent on the SETDB1 methyltransferase, as no H3K9me3 remains at these sites following SETDB1 ablation.

(b) SETDB1 is responsible for H3K9me3 deposition across MORC2 target sites. Considering the genome as a series of 1 kb windows, in this experiment 2978 loci showed a >3-fold reduction in H3K9me3 levels upon disruption of MORC2. Deletion of SETDB1 resulted in a decrease in H3K9me3 at 2918 (98%) of these loci, with 2779 loci (93%) exhibiting a >2-fold reduction.

(c-e) Assessing direct transcriptional targets of the HUSH complex and MORC2. Consistent with a repressive role for MORC2, direct occupancy by MORC2 and/or TASOR was largely restricted to genes that were upregulated rather than downregulated upon MORC2 knockout (c,d). Of the genes upregulated upon MORC2 knockout, around half also exhibited a loss of H3K9me3 and were subject to chromatin decompaction upon loss of MORC2 (e).

(f) Loss of MORC2 does not affect the global expression of genes bound at their TSS by MORC2. The normalized mean expression level of all genes quantified in the RNA-seq experiment displaying HUSH-independent recruitment of V5-MORC2 to their TSS by ChIP-seq (n = 2291 genes) is shown.

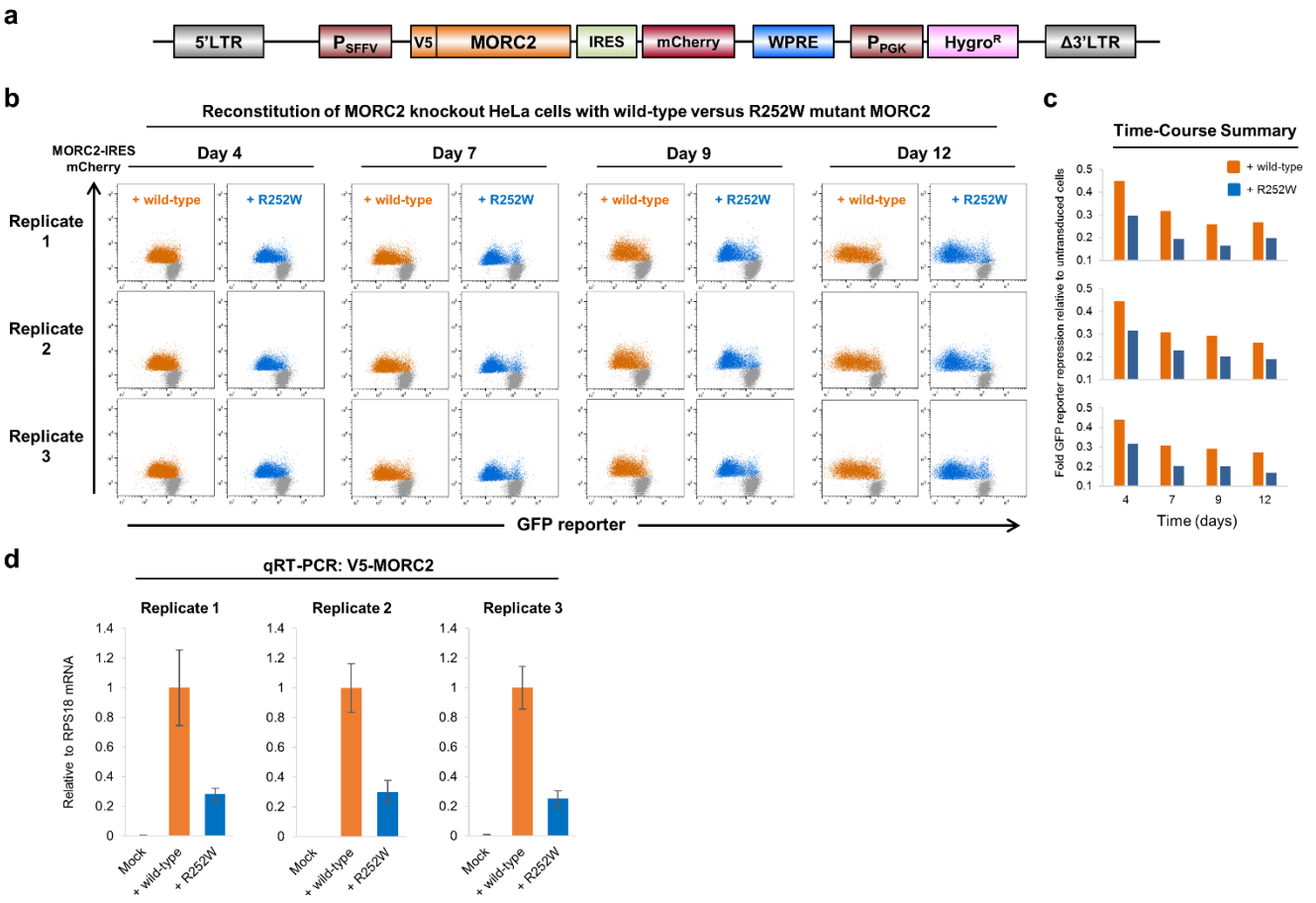

Supplementary Figure 8. The R252W CMT mutation in MORC2 hyper-activates HUSH-mediated transgene repression.

(a) Schematic representation of the MORC2 lentiviral expression vector used. In addition to V5-MORC2, this vector also expresses mCherry from an internal ribosome entry site (IRES) to enable an accurate assessment of the multiplicity of infection achieved.

(b,c) The R252W CMT mutation in MORC2 results in enhanced transgene repression by the HUSH complex. MORC2 knockout HeLa cells harboring a derepressed GFP reporter construct were transduced in triplicate with expression vectors encoding either wild-type of R252W mutant MORC2, such that ~30% of the cells (MOI ~ 1) were transduced (mCherry^{+}) in each case. The restoration of repression of the GFP transgene among the mCherry^{+} populations (colored dots on the histograms) was then followed over the course of 12 days (b), and is quantified in (c).

(d) The R252W CMT mutant exogenous MORC2 construct was expressed at lower levels that the wild-type protein in these experiments, as assessed by qRT-PCR. Error bars indicate the standard deviation of three technical qPCR replicates in each case.

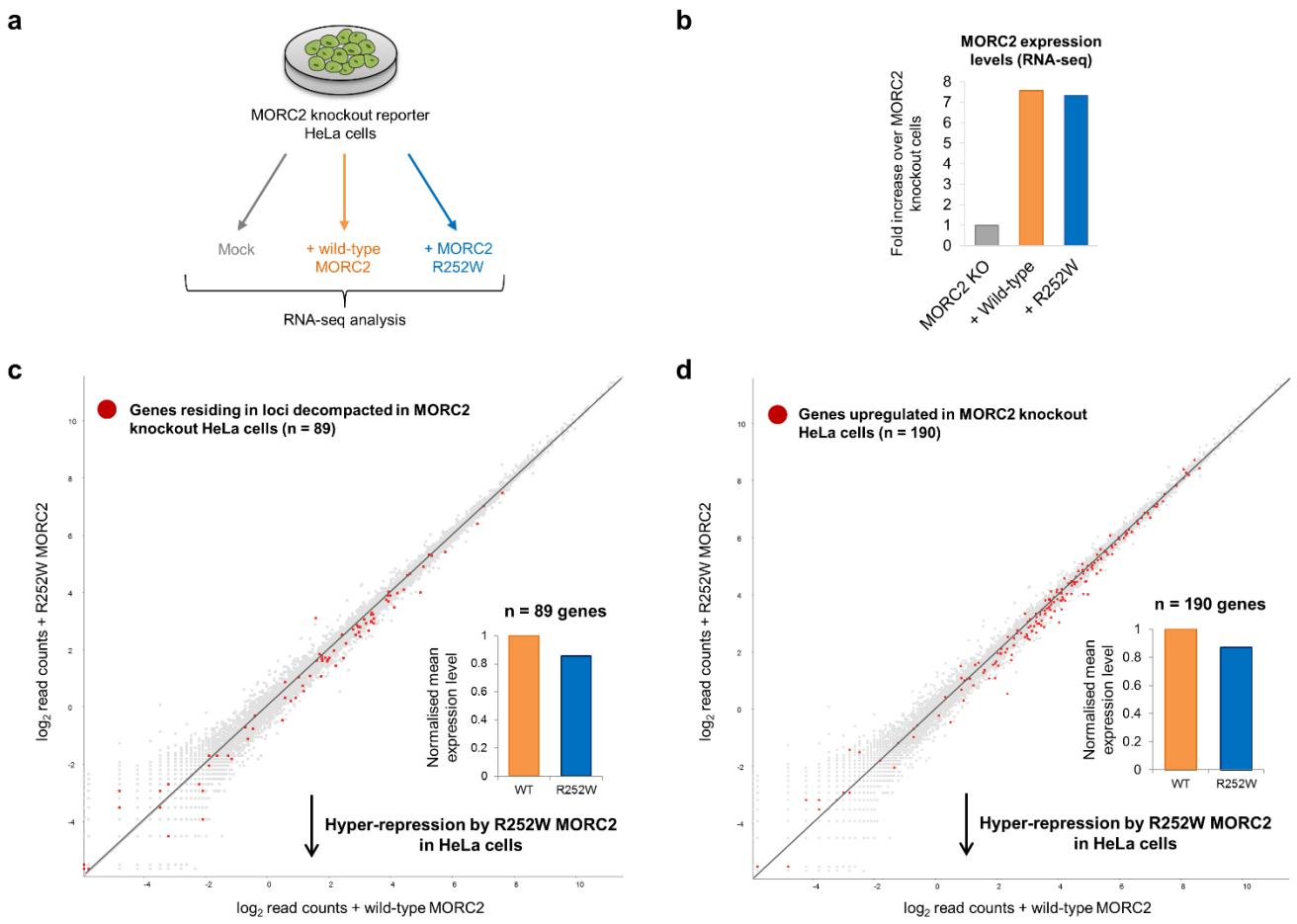

Supplementary Figure 9. Enhanced re-repression of endogenous HUSH target genes upon reconstitution of MORC2 knockout cells with the R252W CMT mutant MORC2.

(a) Schematic representation of the RNA-seq experiment. MORC2 knockout HeLa cells were transduced with lentiviral vectors encoding either wild-type or R252W mutant MORC2, and the re-repression of HUSH target genes was assessed by RNA-seq.

(b) Approximately equal expression of exogenous wild-type and R252W MORC2 mRNA was achieved in this experiment, as assessed by RNA-seq.

(c,d) The R252W mutation in MORC2 results in hyper-repression of HUSH target genes. The red dots highlighted in the scatter plots represent genes residing in loci exhibiting decompaction in MORC2 knockout cells (c) or genes upregulated upon MORC2 knockout (d). Many of the genes in each case lie below the diagonal line y = x, exhibiting reduced transcript levels as a result of hyper-repression by the R252W. The normalized mean expression level across each group of genes is shown in the inset bar charts.

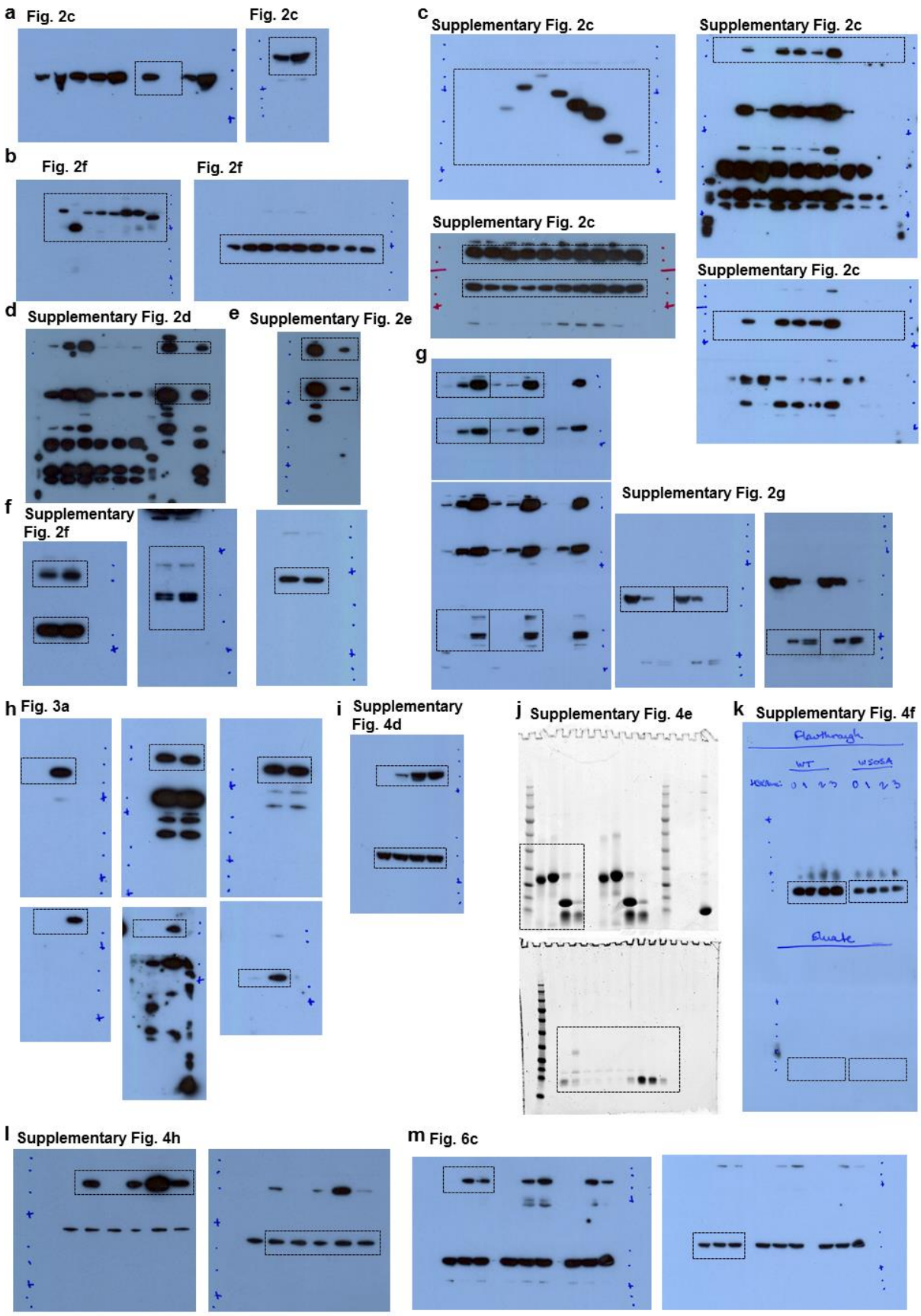

Supplementary Figure 10. Uncropped blot images.

Supplementary References

49. He, F. *et al.* Structural insight into the zinc finger CW domain as a histone modification reader. *Structure* **18,** 1127–39 (2010).

50. Zhang, Q. *et al.* Structure-function analysis reveals a novel mechanism for regulation of histone demethylase LSD2/AOF1/KDM1b. *Cell Res.* **23,** 225–41 (2013).